Thermal evolution of the full three-dimensional magnetic excitations in the multiferroic $BiFeO_3$

Zhijun Xu,[1] Jinsheng Wen,[2,3] Tom Berlijn,[1] Peter M. Gehring,[4] Christopher Stock,[4] M. B. Stone,[5] Wei Ku,[1] Genda Gu,[1] Stephen M. Shapiro,[1] R. J. Birgeneau,[2,3] and Guangyong Xu[1]

[1]*Condensed Matter Physics and Materials Science Department, Brookhaven National Laboratory, Upton, New York 11973, USA*

[2]*Physics Department, University of California, Berkeley, California 94720, USA*

[3]*Materials Science Division, Lawrence Berkeley National Laboratory, Berkeley, California 94720, USA*

[4]*NIST Center for Neutron Research, National Institute of Standards and Technology, Gaithersburg, Maryland 20899, USA*

[5]*Quantum Condensed Matter Division, Oak Ridge National Laboratory, Oak Ridge, Tennessee 37831, USA*

(Received 20 September 2012; published 20 November 2012)

We present neutron inelastic scattering measurements of the full three-dimensional spin-wave dispersion in the multiferroic material $BiFeO_3$ for temperatures from 5 to 700 K. Despite the presence of strong electromagnetic coupling, the magnetic excitations behave as conventional magnons over all parts of the Brillouin zone. At low temperature the spin waves are well-defined coherent modes, described by a classical model for a *G*-type antiferromagnet. A softening of the spin-wave velocity and broadening in energy is already present at room temperature, which is well below the Néel temperature $T_N \sim 640$ K, and increases on heating. In addition, a strong hybridization of the Fe $3d$ and O $2p$ states is found to modify significantly the distribution of the spin-wave spectral weight, which implies that the spins are not restricted to the Fe atomic sites as previously believed.

DOI: 10.1103/PhysRevB.86.174419 PACS number(s): 75.30.Ds, 78.70.Nx, 75.85.+t

I. INTRODUCTION

Coupling between static magnetic and ferroelectric orders in multiferroic materials has attracted tremendous recent interest because of its potential use in device applications.[1–3] If such coupling were to extend to dynamical properties, e.g., between lattice vibrations (phonons) and spin fluctuations (magnons or spin waves), then a new type of excitation may emerge. Those hybrid excitations, or "electromagnons," have already been studied in a number of multiferroic systems using dielectric and Raman measurements.[4–7] This has led to a fascinating idea of embedding and transmitting information within the spin waves,[8,9] with the potential ability to control the spin waves using electric fields generated by low-power dissipating electronic circuits instead of magnetic fields. Possible experimental realizations on the electric field control of electromagnon excitations[7,10] have been tested in $BiFeO_3$, which is one of the most promising functional multiferroic materials.[11]

The coherence of spin waves, which describes how well defined these excitations are, under the influence of the electromagnetic coupling, is of course vital to this process. One of the most significant factors that affects the spin-wave coherence is temperature. Unfortunately, optical measurements such as Raman scattering are only sensitive to long-wavelength excitations. Neutron scattering techniques, on the other hand, provide a powerful means to probe these hybrid excitations over a large momentum space. While there have already been some pioneering neutron scattering measurements on the magnetic excitations from powder[12] and single crystal $BiFeO_3$ samples,[13,14] a quantitative description of the full spectrum at all wave vectors **Q**, and especially their evolution with temperature, is not yet available and highly desired. Here we report neutron inelastic scattering measurements of the full three-dimensional spin-wave dispersion in $BiFeO_3$ for temperatures from 5 to 700 K. The data are normalized to absolute units, so that both the scattering intensity and dispersion can be directly modeled. The spin excitations in $BiFeO_3$ can be reasonably well described by a simple Heisenberg spin Hamiltonian in the antiferromagnetic (AFM) phase. Upon heating the spin-wave modes soften and broaden, indicating that a "decoherence" already starts to occur for T as low as room temperature. A quantitative analysis on the **Q** dependence as well as the total integrated spectral weight also suggests that the local spin structures around Fe sites are not as "local" as generally believed, and a hybridization of the Fe $3d$ and O $2p$ orbitals has to be taken into account as far as the magnetic response is concerned.

$BiFeO_3$ becomes ferroelectric at $T_C \sim 1100$ K. Below T_C this material exhibits an $R3C$ (Refs. 15 and 16) crystal structure, which can be viewed as a (weakly) rhombohedrally distorted perovskite structure in which the oxygen octahedra are also distorted. For the purpose of our magnetic analysis this is well approximated by the pseudocubic unit cell shown in Fig. 1(a). The Néel temperature for $BiFeO_3$ is $T_N \sim 640$ K, and the ordered magnetic phase has a cycloid modulation[17] with a long periodicity that is superimposed on a simple *G*-type antiferromagnetic structure. The magnetic Bragg peaks appear close to the magnetic zone centers of $\mathbf{Q}_{AF} = (0.5,0.5,0.5)$ [reciprocal lattice units (r.l.u.)].

II. EXPERIMENT

Single crystal samples of $BiFeO_3$ were grown using the floating zone technique at Brookhaven National Laboratory (BNL). The crystal used in the measurement has a cylindrical shape, and weighs about 3.5 g, with a mosaic of less than 2°. Neutron inelastic scattering experiments are performed on the wide angular-range chopper spectrometer (ARCS) at the Spallation Neutron Source (SNS) at Oak Ridge National laboratory. Incident energies of 40 and 120 meV were used to probe the lower and higher part of the spin excitation. The single crystal sample was initially aligned so that the neutron beam was incident along the b axis. The crystal was then rotated about the c axis in 2.5° step sizes, covering a total

 ©2012 American Physical Society

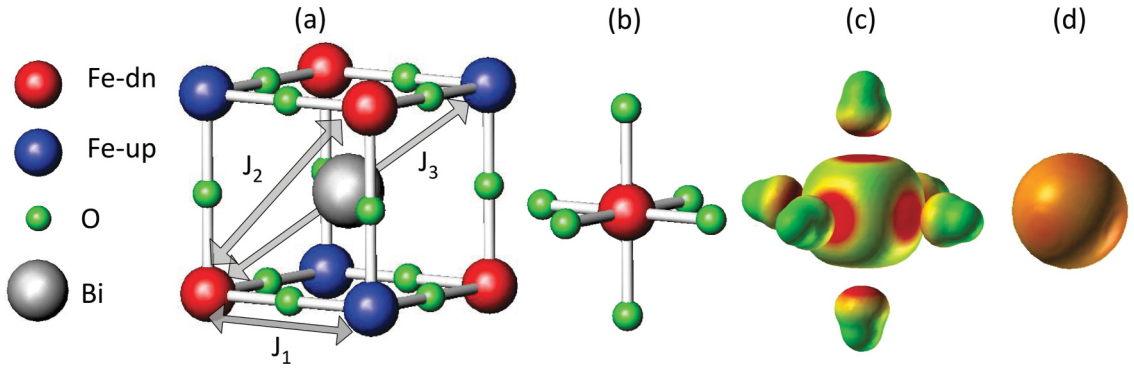


FIG. 1. (Color online) Schematics of the $BiFeO_3$ crystal structure (a), the Fe atom with six Fe-O bonds (b), and spin densities from first principles Wannier analysis taking into account the O *2p* orbital (c), and from conventional Fe ionic model (d). (c) and (d) are plotted on the same scale as in (b).

of 90°, in order to obtain a full coverage on the three-dimensional (3D) reciprocal space.

III. RESULTS AND DISCUSSION

In Figs. 2(a)–2(d), the magnetic excitations measured at $T = 5$ K along [001], [110], [111], and [210] directions

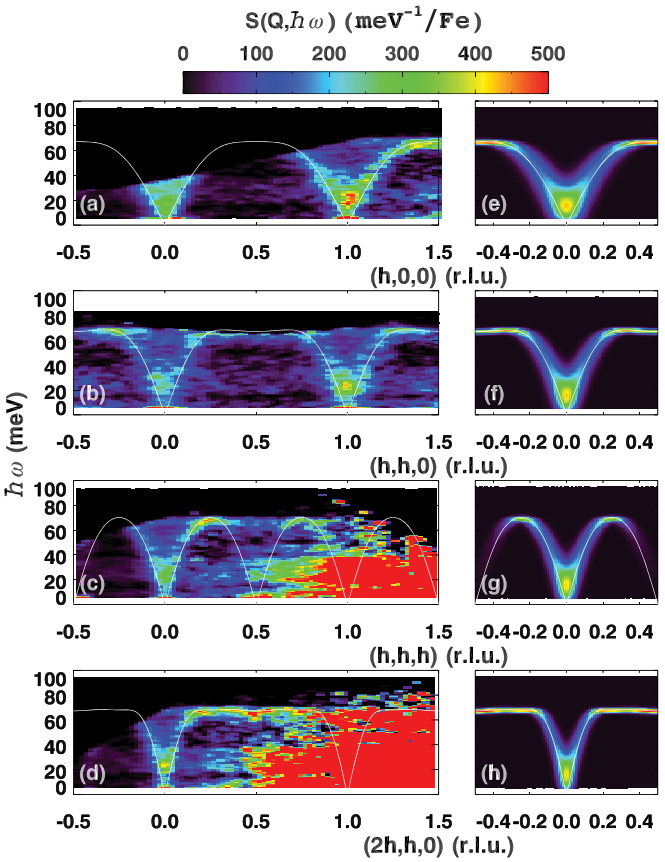


FIG. 2. (Color online) Magnetic excitations from $BiFeO_3$ at $T = 5$ K. The vertical axes denote energy transfer, while the horizontal axes are $\mathbf{Q} - \mathbf{Q}_{AF}$ for $\mathbf{Q}$ along [100], [110], [111], and [210] directions for (a), (b), (c), and (d), respectively. (e)–(h) are model calculations described in the text. The data shown here are measured with $E_i = 120$ meV.

are plotted. At base temperature, the spin-wave excitations are well defined, and disperse quickly when moving away from $\mathbf{Q}_{AF}$. One will see that although the features at higher energies near the top of the bands are very well resolved, fine features at low energies for $\mathbf{Q}$ near $\mathbf{Q}_{AF}$ cannot be accurately determined due to our relatively coarse energy and wave-vector resolution. We then choose to model the magnetic Hamiltonian by ignoring the effect of the long-period cycloid modulation, or any single-ion spin anisotropy in this system, which would only affect[13,14] the magnetic excitations at low energies and in a narrow range around $\mathbf{Q}_{AF} \pm \delta$, where $\delta \sim 0.004$ along $\langle 110 \rangle$ are the modulation wave vectors for the cycloid structure.[18] The Heisenberg spin Hamiltonian of the system therefore can be simplified to that of a classical *G*-type AFM, $H = J \sum_{n,m} \mathbf{S_n} \cdot \mathbf{S_m}$, where we only consider the nearest-neighbor interaction J_1, second-nearest-neighbor interaction J_2, and the third-nearest-neighbor interaction J_3, as shown in Fig. 1(a). The interaction that dominates is clearly the nearest-neighbor exchange interaction J_1 between Fe spins separated along the $\langle 100 \rangle$ direction, whose magnitude can be roughly estimated from the top of the magnetic dispersion band, while J_2 and J_3 can also be obtained if the full dispersion is known.[19,20] We have performed an overall fitting to our data[21,22] to determine the exchange constants and ground state binding energies. The model calculations are shown in Figs. 2(e)–2(h), with fitting parameters shown in Table I. The calculated dispersion curves are also plotted in Fig. 2 as solid lines. It is apparent that our model provides a good description to the data at 5 K. The fact that J_1, J_2, and J_3 are all positive suggests that there is frustration in the system. Specifically, the face-diagonal Fe-Fe spins are ferromagnetically aligned along [110] in spite of the fact that the interactions between them are antiferromagnetic.

Upon heating the spin-wave spectrum is modified gradually. The intensity of low energy magnetic excitations is boosted by the Bose factor from 5 to 140 K and then 300 K, while the overall shape still remain unchanged [see Figs. 3(a)–3(c) and Fig. 4(a)]. This is expected and can be understood as intensities from the magnetic Bragg peak are shifted into the inelastic channels when the static order becomes less robust with heating. At higher energies near the band top, the change is minimal between 5 and 140 K, but at 300 K the band top is noticeably lower [Fig. 3(c) and Figs. 4(c) and 4(d)], and the

TABLE I. Parameters obtained from modeling the data at various temperatures. Note that in our spin Hamiltonian, one pair of spins $\mathbf{S_n}$ and $\mathbf{S_m}$ are counted twice, and their binding energy becomes $H_{nm} = J_{nm}(\mathbf{S_n} \cdot \mathbf{S_m} + \mathbf{S_m} \cdot \mathbf{S_n}) = 2J_{nm}\mathbf{S_n} \cdot \mathbf{S_m}$, so that the exchange constants J used here have the same definition as those used in Ref. 12, but should be compared to half of the J values used in Ref. 13. The units are all meV except for the ordered moment $\langle M_z \rangle$, which is shown as multiples of μ_B.

	5 K	140 K	300 K	580 K	680 K
$\langle M_z \rangle$	3.9(2)	3.6(2)	3.2(3)	1.9(4)	
J_1	2.17(9)	2.17(9)	1.9(1)	1.5(2)	
J_2	0.11(3)	0.11(3)	0.05(5)	0.03(9)	
J_3	0.29(9)	0.29(9)	0.3(2)	0.2(3)	
$2J_1\langle S_0 \cdot S_1 \rangle$	−21(1)	−21(1)	−18(1)	−12(2)	
$2J_2\langle S_0 \cdot S_2 \rangle$	0.26(8)	0.26(8)	0.1(1)	0.1(2)	
$2J_3\langle S_0 \cdot S_3 \rangle$	−2.8(8)	−2.8(8)	−3(1)	−2(2)	
Γ	0	0	5 (2)	10(5)	

excitations become broader in energy [Figs. 4(c) and 4(d)]. The softening and broadening of the spin-wave modes is due to the renormalization that occurs at nonzero temperatures, which is essentially a result of interactions between the excited magnons, and can be modeled with various theories. Instead of going into detail about the renormalization, we still use

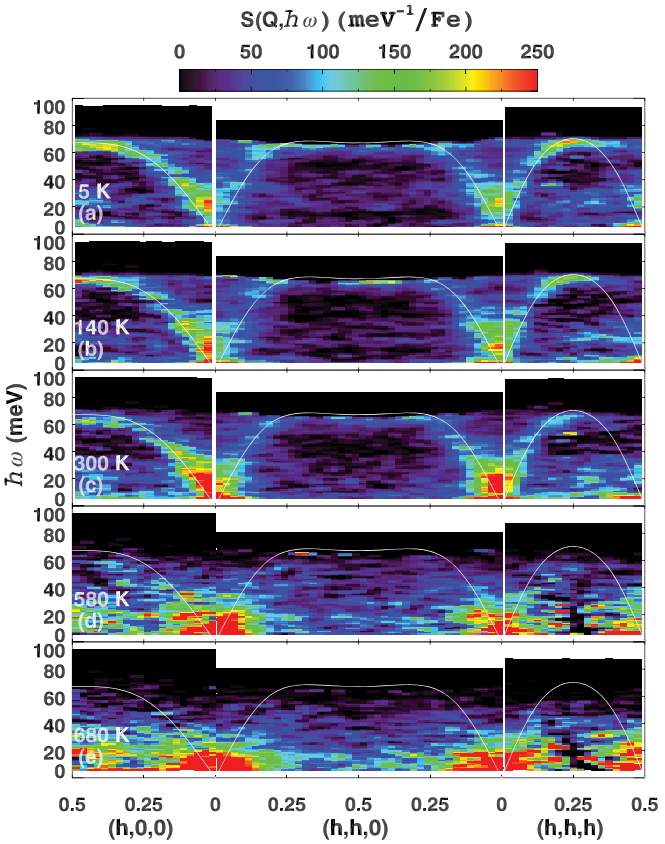


FIG. 3. (Color online) Magnetic excitations from $BiFeO_3$ measured at 5, 140, 300, 580, and 680 K. The horizontal axis denotes $\mathbf{Q} - \mathbf{Q}_{AF}$. The solid lines are dispersion calculated based on parameters obtained from the base temperature (5 K) data. The data shown here are measured with $E_i = 120$ meV.

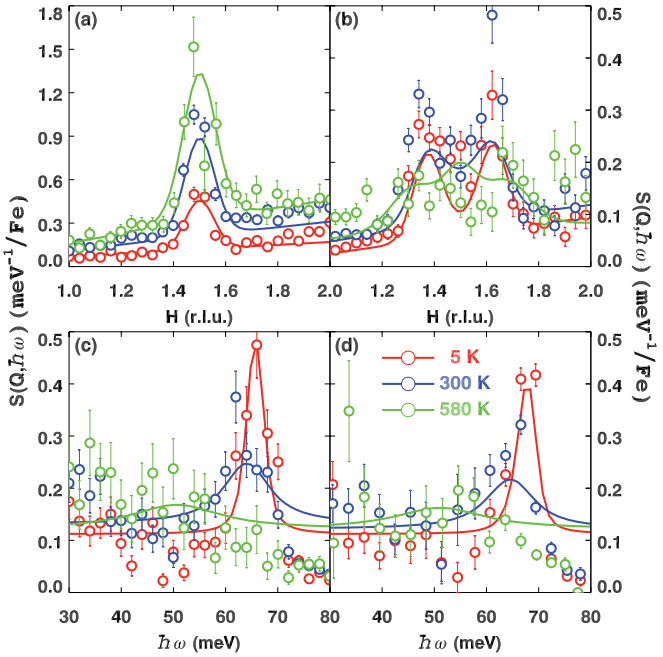


FIG. 4. (Color online) Linear profiles of magnetic excitations from $BiFeO_3$ measured at 5 K (red), 300 K (blue), and 580 K (green). (a) Intensity along $[H,0.5,0.5]$ for $\hbar\omega = 10$ meV, (b) intensity along $[H,0.5,0.5]$ for $\hbar\omega = 40$ meV, (c) an energy cut at $Q = [2,0.5,0.5]$, and (d) an energy cut at $Q = [1.75,0.75,0.75]$. The data shown here are measured with $E_i = 120$ meV. The solid lines are results of model calculations described in the text, including a temperature and Q dependent background to account for phonon contributions.

the same simple spin-wave model that describes the low-T data well, but with a set of renormalized effective exchange parameters shown in Table I. At 140 K the effective exchange parameters are virtually the same as those obtained at 5 K. The effective exchange constants J_1 and J_2 both show a clear drop at $T = 300$ K, and a broadening in energy of $\Gamma \sim 5$ meV is required to obtain a good fit to the data. The solid lines in Fig. 4 are results of the model calculations, which still provide a reasonable description of the data at elevated temperatures.

Our results show that although the spin waves are still relatively well defined at room temperature, the lifetime (inverse of the energy width), or the coherence, of the spin-wave mode does decrease significantly compared to that at base temperature. The magnitude of the spin-wave softening is smaller than the softening observed of the electromagnon modes[5] by Raman measurements near $q = 0$, but note that the energy of the $q = 0$ mode in the Raman work is also related to the cycloid wave vector[23] δ, which also drops with heating.[18] The clear velocity softening and reduction of spin-wave coherence at 300 K makes the low temperature measurements important to obtain the ground state values of the exchange constants and related parameters.

With further heating towards $T_N \sim 640$ K, the spin waves become heavily damped, as shown in Figs. 3(d) and 3(e). The data taken at 580 K already show that although the scattered intensities are more intense around $\mathbf{Q}_{AF}$ due to the dominating AFM correlations, well-defined spin waves are no longer

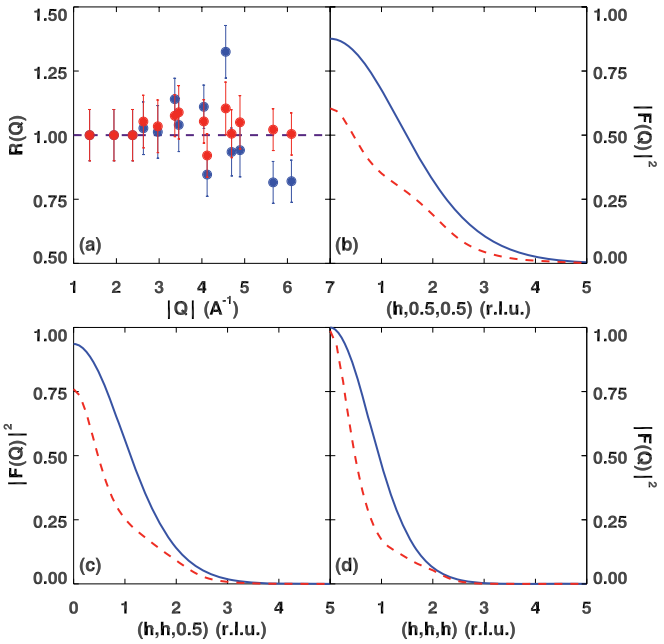


FIG. 5. (Color online) Comparison of the original ionic Fe form factor and the new Wannier form factor. (a) Plot of the ratio $R(\mathbf{Q}) = \frac{I(\mathbf{Q})/|F(\mathbf{Q})|^2}{I(\mathbf{Q}_0)/|F(\mathbf{Q}_0)|^2}$, where $I(\mathbf{Q})$ is magnetic scattering intensity measured at wave vector $\mathbf{Q}$, while $\mathbf{Q}_0$ is the wave vector equivalent to $\mathbf{Q}$ in the first Brillouin zone. Ideally this value should be 1 (see the dashed line). The red symbols are values calculated using the new Wannier form factor while the blue symbols using the old Fe ionic form factor. The data are selected from measurements with $E_i = 40$ and 120 meV, taken at $T = 5$ K. The error bars are derived from the error bars of the data being used. (b)–(d) $|F(\mathbf{Q})|^2$ plotted along different directions.

present, and the deviation from model calculations to the measured data starts to become more pronounced (see Fig. 4). While the Néel temperature marks the disappearance of static magnetic order in the system, the coherence of spin-wave excitations already diminishes at temperatures well below T_N.

In addition to probing the coherence of the spin-wave excitations, which are collective magnetic responses from the system, our neutron scattering measurements also provide information on the local spin structure around each Fe atom. The magnetic form factor $|F(\mathbf{Q})|^2$ describes the Fourier transformation of the spatial distribution of spin (density) around each magnetic ion (in our case, Fe^{3+}) into momentum space. In Figs. 5(b)–5(d), we show the magnetic form factor for a Fe^{3+} ion with the blue solid lines. This magnetic form factor is isotropic and only depends on the length of $\mathbf{Q}$. However, a recent analysis of inelastic neutron scattering data from high-T_C cuprates suggests[24] that the spin distribution around magnetic ions in metal oxides can be greatly affected by the presence of the oxygen ion, and could result in different effective magnetic form factors.

To compute the magnetic form factor that includes the effects of the crystalline environment, a first principles Wannier analysis[24,25] is employed. Local density approximation plus Hubbard U (LDA + U) calculations of $BiFeO_3$ (Refs. 26 and 27) show that the Fe cation is in the high-spin $S = 5/2$ state. The magnetic form factor is obtained by Fourier transforming the spin density of the low-energy Wannier functions of Fe. In Figs. 1(c) and 1(d), we compare the atomic spin density with the Wannier function derived spin density. The main difference is that the Wannier function derived spin density spreads into the neighboring oxygen atoms, which suppresses the magnetic form factor at nonzero momenta. Direct comparisons of the form factors are plotted in Figs. 5(b)–5(d). We can see that for most Q, the Wannier form factor is smaller than the previously used ionic form factor. An experimental verification of the new form factor is shown in Fig. 5(a). Here we plot the ratio $R(\mathbf{Q}) = \frac{I(\mathbf{Q})/|F(\mathbf{Q})|^2}{I(\mathbf{Q}_0)/|F(\mathbf{Q}_0)|^2}$, where $I(\mathbf{Q})$ is magnetic scattering intensity measured at wave vector $\mathbf{Q}$, while $\mathbf{Q}_0$ is the wave vector equivalent to $\mathbf{Q}$ in the first Brillouin zone. It is also worth noting that this type of calculation is model (Hamiltonian) independent, and $R(\mathbf{Q})$ is supposed to always be 1 if the magnetic form factor used is correct. The results from the old ionic (blue symbols) and new Wannier (red symbols) magnetic form factors clearly suggest that the new form factor provides a better description of the $\mathbf{Q}$ dependence.

Using this hybrid magnetic form factor, the ordered moment per Fe at various temperatures is calculated and listed in the first row of Table I. At $T = 5$ K, this value $M_z = 4\mu_B$ corresponds to $S_Z = 2.0$, consistent with the moment obtained from other measurements,[28,29] and close to the theoretical limit of $S_Z = S = 5/2$, using a g factor of 2. Frustration due to a positive (AFM) J_2 is likely the main reason for the difference. We can also obtain an integrated spectral weight from all of the spin-wave excitations, which turns out to be $S_{\text{dynamic}} \sim 2.5$ (i.e., $M^2_{\text{dynamic}} = S_{\text{dynamic}} g^2 \mu_B^2 = 10\mu_B^2$). Combining the two we have a total squared moment of $M^2 = M_z^2 + M^2_{\text{dynamic}} = 16 + 10 = 26\mu_B^2$, which is supposed to be $S(S+1)g^2\mu_B^2$ to satisfy the sum rule.[22] This corresponds to $S \sim 2.1$ per Fe, in good agreement with the expected $S = 5/2$ from Fe^{3+}. On the other hand, if a simple Fe^{3+} magnetic form factor were used, we would have obtained a $S_Z = 1.4$ and $S = 1.4$ instead, which are much lower than the expected values.

IV. SUMMARY

Overall, our work demonstrates that the magnetic excitations in $BiFeO_3$ can be very well modeled with a simple spin-wave model from a G-type AFM at low temperature. Despite the cycloid modulation induced by coupling to the electric polarization, most of the spin dynamics is barely modified, and consistent with the behavior of a conventional spin wave. No extra electromagnon modes[5] are observed near magnetic zone boundaries (i.e., the long-wavelength limit), which is likely due to the relative small neutron cross sections for the AFM-type spin excitation at long wavelengths. Upon heating decoherence of spin-wave excitations starts to occur even at just below room temperature (300 K). At 580 K, which is well below T_N, the coherence mode is already almost completely destroyed. In addition, a strong hybridization between the Fe and O orbitals needs to be taken into account when the magnetic response is considered. Even as a good insulator, the electrons responsible for the magnetic moments are not restricted at the Fe sites, and the local magnetic moment could extend well beyond the typical ionic radius of Fe^{3+} into the adjacent O^{2-} sites.

ACKNOWLEDGMENTS

Z.J.X., T.B., W.K., G.D.G., S.M.S., and G.Y.X. acknowledge support by the Office of Basic Energy Sciences, US Department of Energy under Contract No. DE-AC02-98CH10886. J.W. and R.J.B. are supported by the same office through Contract No. DE-AC02-05CH11231. This research at ORNL's Spallation Neutron Source was sponsored by the Scientific User Facilities Division, Office of Basic Energy Sciences, US Department of Energy.

[1] J. F. Scott, Nat. Mater. **6**, 256 (2007).

[2] W. Eerenstein, N. D. Mathur, and J. F. Scott, Nature (London) **442**, 759 (2006).

[3] S.-W. Cheong and M. Mostovoy, Nat. Mater. **6**, 13 (2007).

[4] A. Pimenov, A. A. Mukhin, V. Y. Ivanov, V. D. Travkin, A. M. Balbashov, and A. Loidl, Nat. Phys. **2**, 97 (2006).

[5] M. Cazayous, Y. Gallais, A. Sacuto, R. de Sousa, D. Lebeugle, and D. Colson, Phys. Rev. Lett. **101**, 037601 (2008).

[6] A. Kumar, N. M. Murari, and R. S. Katiyara, Appl. Phys. Lett. **92**, 152907 (2008).

[7] P. Rovillain, R. de Sousa, Y. Gallais, A. Sacuto, M. A. Measson, D. Colson, A. Forget, M. Bibes, A. Barthelemy, and M. Cazayous, Nat. Mater. **9**, 975 (2010).

[8] V. V. Kruglyak, S. O. Demokritov, and D. Grundler, J. Phys. D: Appl. Phys. **43**, 264001 (2010).

[9] Y. Kajiwara, K. Harii, S. Takahashi, J. Ohe, K. Uchida, M. Mizuguchi, H. Umezawa, H. Kawai, K. Ando, K. Takanashi, S. Maekawa, and E. Saitoh, Nature (London) **464**, 262 (2010).

[10] A. Kumar, J. F. Scott, and R. S. Katiyar, Appl. Phys. Lett. **99**, 062504 (2011).

[11] G. Catalan and J. F. Scott, Adv. Mater. **21**, 2463 (2009).

[12] O. Delaire, M. B. Stone, J. Ma, A. Huq, D. Gout, C. Brown, K. F. Wang, and Z. F. Ren, Phys. Rev. B **85**, 064405 (2012).

[13] J. Jeong, E. A. Goremychkin, T. Guidi, K. Nakajima, G. S. Jeon, S.-A. Kim, S. Furukawa, Y. B. Kim, S. Lee, V. Kiryukhin, S.-W. Cheong, and J.-G. Park, Phys. Rev. Lett. **108**, 077202 (2012).

[14] M. Matsuda, R. S. Fishman, T. Hong, C. H. Lee, T. Ushiyama, Y. Yanagisawa, Y. Tomioka, and T. Ito, Phys. Rev. Lett. **109**, 067205 (2012).

[15] A. Palewicz, R. Przenioslo, I. Sosnowska, and A. W. Hewat, Acta Crystallogr., Sect. B **63**, 537 (2007).

[16] A. Palewicz, I. Sosnowska, R. Przenioslo, and A. W. Hewat, Acta Phys. Pol., A **117**, 296 (2010).

[17] I. Sosnowska, T. P. Neumaier, and E. Steichele, J. Phys. C **15**, 4835 (1982).

[18] M. Ramazanoglu, W. Ratcliff, Y. J. Choi, S. Lee, S. W. Cheong, and V. Kiryukhin, Phys. Rev. B **83**, 174434 (2011).

[19] I. Zaliznyak, in *Handbook of Magnetism and Advanced Magnetic Materials*, edited by H. Kronmüller and S. Parkin (Wiley, Hoboken, NJ, 2007), Vol. 3, Chap. 20.

[20] The spin-wave calculations are based on a classical spin-wave model assuming a $S = 5/2$ G-type AFM. Based on the model, the values of J_1, J_2, and J_3 can all be directly derived from the data if the energies of the spin-wave excitations can be accurately determined at each wave vector. For instance, if we define $\mathbf{Q}_1 = \mathbf{Q}_{\mathrm{AF}} + (0.25,0.25,0)$, $\mathbf{Q}_2 = \mathbf{Q}_{\mathrm{AF}} + (0.25,0.25,0.25)$, $\mathbf{Q}_3 = \mathbf{Q}_{\mathrm{AF}} + (0.5,0.25,0)$, based on a simple spin-wave calculation, we have $J_1 = \frac{1}{4S}(E_2^2 - E_1^2)^{1/2}$, $J_2 = \frac{1}{8S}(E_2 - E_3)$, and $J_3 = \frac{1}{4}(\frac{E_3}{4S} - 3J_1 + 8J_2)$. Here E_1, E_2, and E_3 are spin-wave energies at $\mathbf{Q}_1$, $\mathbf{Q}_2$, and $\mathbf{Q}_3$, respectively.

[21] I. Zaliznyak and S.-H. Lee, in *Modern Techniques for Characterizing Magnetic Materials*, edited by Y. Zhu (Springer, Heidelberg, 2005), Chap. 1.

[22] After normalizing the data using phonon intensities which have been obtained from the same measurements, a sum rule applies: $\int_{\mathrm{BZ}} \int S(\mathbf{Q},\hbar\omega) d^3\mathbf{Q} d(\hbar\omega) / \int_{\mathrm{BZ}} d^3\mathbf{Q} = S(S+1)$, where $S(\mathbf{Q},\hbar\omega)$ is the dynamic spin correlation function, and the integral is performed in one Brillouin zone. In our case $I(\mathbf{Q},\hbar\omega) = \frac{2}{3} S(\mathbf{Q},\hbar\omega)$, where $I(\mathbf{Q},\hbar\omega)$ is the normalized intensity. The factor $\frac{2}{3}$ arises from assuming an isotropic dynamic spin correlation function (i.e., $S^{xx} = S^{yy} = S^{zz}$), and averaging the polarization factor of different domains. The scattering intensity can be modeled with the single mode approximation (SMA), and the parameters that can vary include the exchange parameters J_1, J_2, J_3, ground state binding energies for the nearest, second-nearest (face diagonal), and third-nearest (body diagonal) spin pairs, $2J_1\langle S_0 S_1\rangle$, $2J_2\langle S_0 S_2\rangle$, $2J_3\langle S_0 S_3\rangle$, and a finite energy broadening Γ for high temperature data.

[23] R. de Sousa and J. E. Moore, Phys. Rev. B **77**, 012406 (2008).

[24] A. C. Walters, T. G. Perring, J.-S. Caux, A. T. Savici, G. D. Gu, C.-C. Lee, W. Ku, and I. A. Zaliznyak, Nat. Phys. **5**, 867 (2009).

[25] W. Ku, H. Rosner, W. E. Pickett, and R. T. Scalettar, Phys. Rev. Lett. **89**, 167204 (2002).

[26] We applied the WIEN2K implementation of the all-electron linearized augmented plane wave method in the LDA + U approximation using $U = 4$ eV and $J = 0.9$ eV. The basis size was determined by $\mathrm{RK}_{\mathrm{max}} = 7.0$ and the Brillouin zone was sampled with a $7 \times 7 \times 7$ mesh.

[27] K. Schwarz, P. Blaha, and G. Madsen, Comput. Phys. Commun. **147**, 71 (2002).

[28] P. Fischer, M. Polomska, I. Sosnowska, and M. Szymanski, J. Phys. C **13**, 1931 (1980).

[29] I. Sosnowska, R. Przenios, P. Fischer, and V. A. Murashov, J. Magn. Magn. Mater. **160**, 384 (1996).